energies

MDPI

Article

Defect, Diffusion and Dopant Properties of $NaNiO_2$: Atomistic Simulation Study

Ruwani Kaushalya [1], Poobalasuntharam Iyngaran [1], Navaratnarajah Kuganathan [2,3,*] and Alexander Chroneos [2,3]

1 Department of Chemistry, University of Jaffna, Sir. Pon Ramanathan Road, Thirunelvely, Jaffna 40000, Srilanka
2 Department of Materials, Imperial College London, London SW7 2AZ, UK
3 Faculty of Engineering, Environment and Computing, Coventry University, Priory Street, Coventry CV1 5FB, UK
* Correspondence: n.kuganathan@imperial.ac.uk or ad0636@coventry.ac.uk

Received: 23 June 2019; Accepted: 8 August 2019; Published: 12 August 2019

Abstract: Sodium nickelate, $NaNiO_2$, is a candidate cathode material for sodium ion batteries due to its high volumetric and gravimetric energy density. The use of atomistic simulation techniques allows the examination of the defect energetics, Na-ion diffusion and dopant properties within the crystal. Here, we show that the lowest energy intrinsic defect process is the Na-Ni anti-site. The Na Frenkel, which introduces Na vacancies in the lattice, is found to be the second most favourable defect process and this process is higher in energy only by 0.16 eV than the anti-site defect. Favourable Na-ion diffusion barrier of 0.67 eV in the *ab* plane indicates that the Na-ion diffusion in this material is relatively fast. Favourable divalent dopant on the Ni site is Co^{2+} that increases additional Na, leading to high capacity. The formation of Na vacancies can be facilitated by doping Ti^{4+} on the Ni site. The promising isovalent dopant on the Ni site is Ga^{3+}.

Keywords: $NaNiO_2$; defects; Na diffusion; dopants; atomistic simulation

1. Introduction

In the field of energy storage, a significant amount of research activity has been devoted to Li-ion batteries [1–10]. As the global distribution of lithium is limited and inhomogeneous, there is a necessity to find an alternative to the lithium ion battery for the next-generation of high capacity energy storage systems, particularly in the hybrid electric vehicles.

Rechargeable sodium ion batteries have become promising for the application in large-scale energy storage devices due to the remarkable abundance of sodium on the earth. The performance of a sodium ion battery (SIB) relies on several factors. Developing cathode materials exhibiting cheap, safe and high energy density is one of the key steps for constructing promising rechargeable SIBs. A variety of sodium-based cathode materials have been examined experimentally and a limited number of theoretical works have been reported in the literature [4,5,11–20]. For portable applications, a few of them can be promising as the ionic radius of Na is much larger than the ionic radius of Li. Larger size of Na will also affect Na^+ ion intercalation and diffusion leading to degradation in the specific capacity and rate capacity [21]. Electrochemical stability would be difficult due to the volume expansion caused by Na^+ insertion. Furthermore, low potential and large atomic weight of Na lead to the specific energy reduction in the battery [4].

Several promising cathode materials including Olivine $NaMPO_4$ (M = Fe, Mn, Co, Ni), Maricite $NaMPO_4$ (M = Fe, Mn, Co, Ni), NASICON (Natrium SuperIonic CONductor) $Na_3V_2(PO_4)_3$ and Layered Na_xMO_2 (M = Fe, Mn, Co, Ni) were proposed for Na-ion batteries [22,23]. The research

activity on the Olivine $NaMPO_4$ is due to the commercial use of $LiFePO_4$ as cathode material for Li-ion batteries [22]. The Maricite $NaMPO_4$ was also considered as potential cathode materials due to their high thermodynamical stability. The NASICON family of compounds have been extensively studied as Na-ion battery cathodes due to their three-dimensional framework and large interstitial channels [22].

The "Layered" $NaMO_2$ (M = Fe, Mn, Co, Ni) structures have received considerable attention for their use as potential cathode materials in Na-ion batteries due to their high volumetric and gravimetric energy densities [24–28]. Miyazaki et al. [27] reported the synthesis of monoclinic $NaNiO_2$ and tested this compound as a cathode material. Their study shows that initial open circuit voltage is 2.47 V and only 0.2 Na can be extracted during the first cycle. Later Vassilaras et al. [28] re-investigated this material and noted that there is an improvement in the initial open circuit voltage. Furthermore, the quantities of Na de-intercalated and intercalated were reported to be 0.85 and 0.62 respectively and their corresponding discharge and charge capacities were 147 mAh/g and 199 mAh/g. Good structural stability was also noted for more than 20 cycles.

As there is a limited number of experimental reports available in the literature, further understanding of this material is necessary to optimize its performance in Na-ion batteries. Computational studies at the atomistic level can provide information on intrinsic defect energetics, ion migration and dopant substitution [29–48]. To the best of our knowledge, there is no work reported related to defect and diffusion properties of $NaNiO_2$. Here we attempt to examine the defect structures, Na-ion diffusion pathways and isovalent and aliovalent dopants in $NaNiO_2$ by performing classical potential simulations. This well-established simulation method has been applied to numerous oxide materials including battery materials [29–48].

2. Computational Methods

Classical pair-wise potential calculations for the bulk and defective $NaNiO_2$ structures were carried out using the General Utility Lattice Program (GULP) code [49]. In this method, total energy (lattice energy) of the system is calculated using long range (Coulombic) and short range (electron-electron repulsive and attractive intermolecular forces). Buckingham potentials (refer to Supplementary Materials) were used to model short range forces. Full structural relaxations (both ion positions and lattice constants) were performed using the Broyden-Fletcher-Goldfarb-Shanno (BFGS) algorithm [50]. In all relaxed configurations, forces on each atoms were <0.001 eV/Å. Point defects were modelled using the Mott-Littleton method [51]. Full charge with spherical shape of ions at dilute limit can overestimate the defect formation enthalpies. Nevertheless, the trend will be the same. Isobaric parameters were used in the present simulation to calculate the formation and migration energies. In our previous theoretical work, we have discussed the detailed thermodynamic relations associated with isobaric parameters [52–54].

3. Results

3.1. Crystal Structure of $NaNiO_2$

$NaNiO_2$ structure crystallizes in the monoclinic C2/m space group, having lattice parameters a = 5.3222 Å, b = 2.8458 Å, c = 5.5832 Å, $\alpha = \gamma = 90.0°$ and $\beta = 110.47°$ [28]. Figure 1 exhibits the experimentally observed crystal structure of $NaNiO_2$. This structure has layers of edge-sharing NiO_6 octahedra units. The Na ions lie between the layers forming distorted octahedra.

Equilibrium lattice constants were obtained by performing full geometry optimisation (both ion positions and lattice constants). The calculated lattice constants are reported in Table 1. There is a good agreement between the expertiment and calculation ensuring the choice of potentials used in this study.

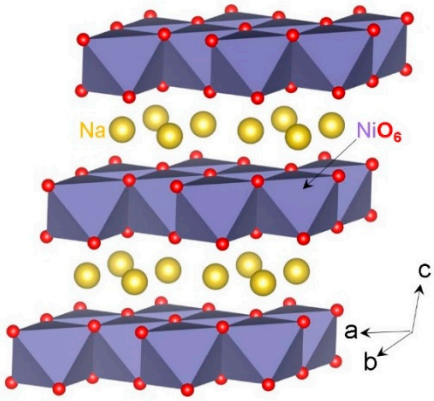

Figure 1. Crystal structure of monoclinic-$NaNiO_2$ (space group *C*/2m).

Table 1. Calculated structural parameters and corresponding experimental values [28] reported for monoclinic (*C*/2m) $NaNiO_2$.

Parameter	Calc.	Exp. [28]	|Δ|(%)
a (Å)	5.1097	5.3222	3.99
b (Å)	2.9501	2.8458	3.66
c (Å)	5.6092	5.5832	0.46
$\alpha = \gamma$ (°)	90.0	90.0	0.00
β (°)	107.68	110.47	2.52
V (Å^3)	80.56	79.22	1.69

3.2. Intrinsic Defect Processes

Intrinsic defects play an important role in the migration of ions in materials. Here we considered point defects in the form of vacancies, interstitials, and anti-sites. They were then combined to calculate formation energies for Frenkel and Schottky defects. Anti-site defect energies were calculated by interchanging the cations (Ni on Na and Na on Ni). The reaction energies for those defects are written by using Kröger-Vink notation [55].

$$\text{Na Frenkel}: \ \mathrm{Na}^{X}_{Na} \rightarrow V'_{Na} + \mathrm{Na}^{\bullet}_{i} \tag{1}$$

$$\text{Ni Frenkel}: \ V^{X}_{Ni} \rightarrow V'''_{Ni} + \mathrm{Ni}^{\bullet\bullet\bullet}_{i} \tag{2}$$

$$\text{O Frenkel}: \ \mathrm{O}^{X}_{O} \rightarrow V^{\bullet\bullet}_{O} + \mathrm{O}''_{i} \tag{3}$$

$$\text{Schottky}: \ \mathrm{Na}^{X}_{Na} + \mathrm{Ni}^{X}_{Ni} + 2\,\mathrm{O}^{X}_{O} \rightarrow V'_{Na} + V'''_{Ni} + 2\,V^{\bullet\bullet}_{O} + \mathrm{NaNiO_2} \tag{4}$$

$$\mathrm{Na_2O}\ \text{Schottky}: 2\mathrm{Na}^{X}_{Na} + \mathrm{O}^{X}_{O} \rightarrow 2\,V'_{Na} + V^{\bullet\bullet}_{O} + \mathrm{Na_2O} \tag{5}$$

$$\text{Na/Ni antisite (isolated)}: \ \mathrm{Na}^{X}_{Na} + \mathrm{Ni}^{X}_{Ni} \rightarrow \mathrm{Na}''_{Ni} + \mathrm{Ni}^{\bullet\bullet}_{Na} \tag{6}$$

$$\text{Na/Ni antisite (cluster)}: \ \mathrm{Na}^{X}_{Na} + \mathrm{Ni}^{X}_{Ni} \rightarrow \left\{\mathrm{Na}''_{Ni} : \mathrm{Ni}^{\bullet\bullet}_{Na}\right\}^{X} \tag{7}$$

Figure 2 shows the defect reaction energies per defect. The present calculations show that the Na-Ni anti-site defect cluster is the most favourable defect (1.86 eV). This suggests that there is a possibility of a small amount of Na on Ni sites (Na''_{Ni}) and Ni on Na sites ($\mathrm{Ni}^{\bullet\bullet}_{Na}$). This defect has been identified theoretically as a most promising defect in a variety of oxide materials [31–42]. During the preparation of as-prepared battery materials and the charge-discharge process, the presence of this defect was noted [35,56–59]. The Na Frenkel is the second most thermodynamically favourable defect process and the defect energy is only 0.16 eV higher than the anti-site defect energy. In the Na Frenkel process, Na vacancies would be created and this process would facilitate vacancy mediated

Na-ion diffusion in $NaNiO_2$. The reaction energy for the formation of Na_2O Schottky (relation 5) is 2.16 eV/defect. This process is also competitive as the defect energy is close to the defect energy calculated for the anti-site and the Na Frenkel. The formation of further V'_{Na} and $V_O^{\bullet\bullet}$ can be enhanced by the Na_2O Schottky process at moderate temperatures.

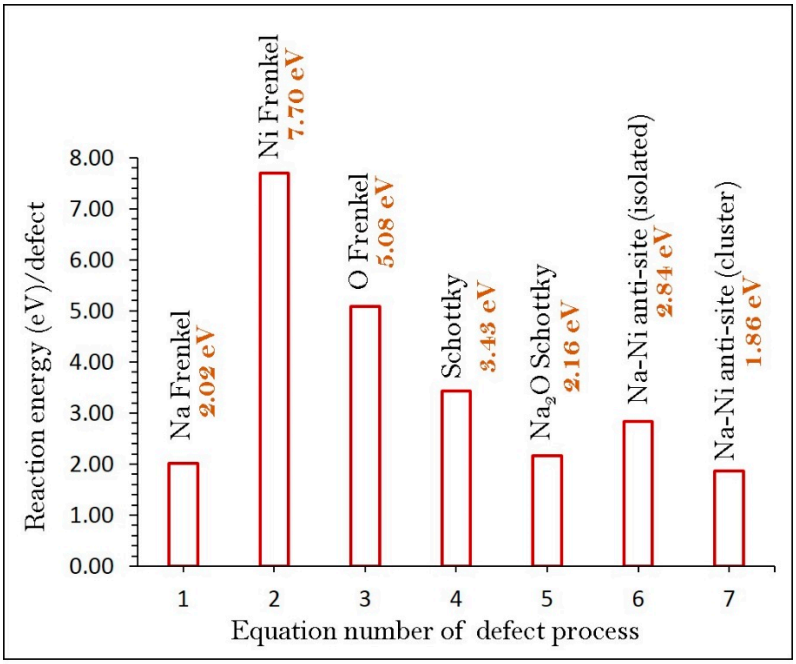

Figure 2. Energetics of intrinsic defect process calculated in monoclinic $NaNiO_2$.

3.3. Sodium Ion Diffusion

As Na-ion diffusion rate strongly influences the cathode performance, it is necessary to examine the sodium ion diffusion pathways together with activation energies. Experimental characterisation of diffusion pathways can be quite challenging. Current simulation techniques enabled us to identify the Na-ion diffusion pathways with activation energies at the atomic level. We identified a promising Na local hop with the Na-Na seperation of 2.95 Å. Its activation energy of migration is calculated to be 0.67 eV. Figure 3 shows the long range Na-ion difussion pathway constructed by connecting local Na hops and the corresponding energy profile diagram for the local Na hop.

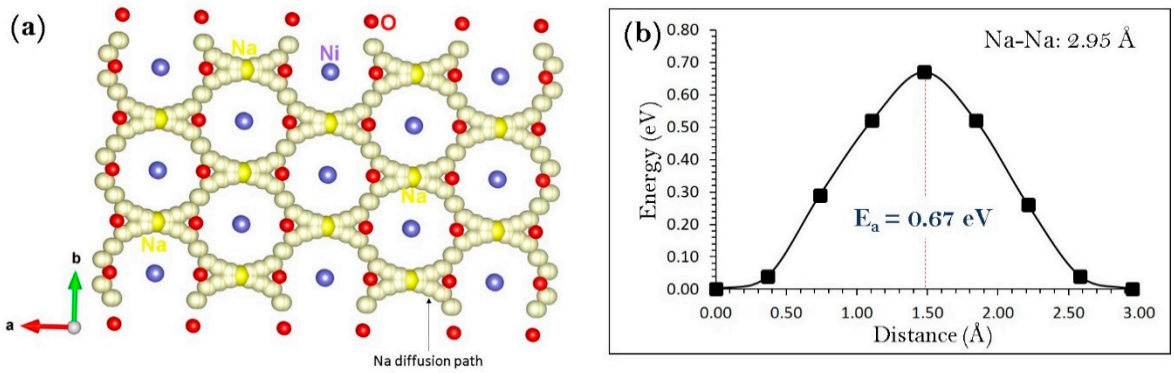

Figure 3. (**a**) Long-range sodium-ion diffusion path constructed using Na local hops and (**b**) energy profile diagram for the Na local hop.

The long range Na-ion diffusion pathway is in the *ab* plane exhibiting a non-linear pattern with overall activation energy of 0.67 eV. The present simulation results show that Na-ion diffusion will be significant in this material.

3.4. Solution of Divalent Dopants

Additional Na in the as-prepared $NaNiO_2$ material would increase the capacity and the rate of Na-ion diffusion. The later is due to the shorter Na-Na distances arising from additional Na in the material than those present in the defect-free structure. Divalent doping on the Ni site is a promising stratergy to introduce Na interstitials as explained in the equation 8. A similar stratergy was applied to Li, Na, and Mg-ion battery materials in our previous theoretical studies [36–47]. The solution of MO (M = Mg, Co, Fe, Ca, Sr and Ba) was considered using the following reaction:

$$2MO + 2Ni_{Ni}^{X} + Na_2O \rightarrow 2M'_{Ni} + 2\,Na_i^{\bullet} + Ni_2O_3 \quad (8)$$

Solution enthalpies are reported in Figure 4. In all cases solution enthalpies are endoergic suggesting that this process should be carried out under thermal condition. The lowest solution enthalpy is calculated for Co^{2+}(3.89 eV). It should be noted that the solution enthalpies of MgO (3.93 eV) and FeO (4.00 eV) are closer to the values calculated for CoO indicating that Mg^{2+} and Fe^{2+} are also candidate dopants. The possible formula for the Co-doped composite is $NaCo_xNi_{1-x}O_2$ ($0.00 < x < 1.00$). The exact value of x can be determined by experiments. There is a gradual increase in the solution enthalpies from Ca to Ba. Solution enthalpies of CaO and SrO are 5.01 eV and 7.36 eV respectively. Solution enthalpy of BaO is highly positive (~10 eV) meaning that this process cannot be executed at operating temperatures.

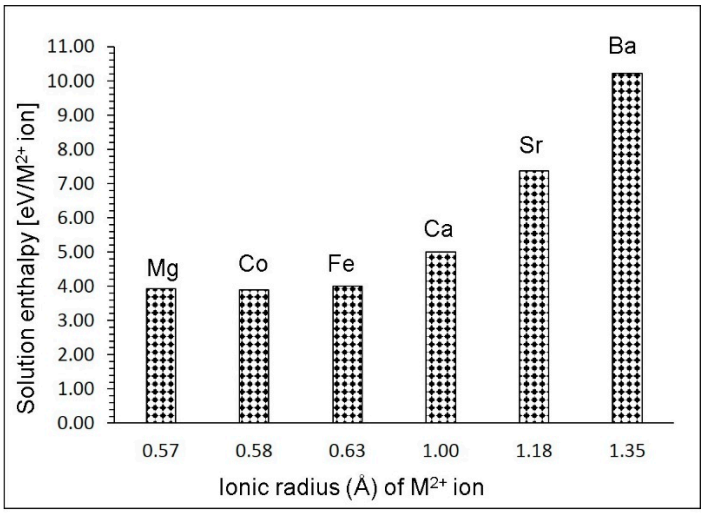

Figure 4. Solution enthalpies of divalent dopants at the Ni site with respect to ionic radii.

3.5. Solution of Trivalent Dopants

Here, a wide range of trivalent dopants (M = Al, Ga, Fe, In, Sc, Y, Gd, and La) were considered at the Ni site. These dopants are isovalent to Ni because the oxidation state of Ni in $NaNiO_2$ is +3. Isovalent doping process is important as it can control the point defects and tune the electronic properties of this material. The following reaction equation was used to calculate the solution enthalpy.

$$M_2O_3 + 2Ni_{Ni}^{X} \rightarrow 2M_{Ni}^{X} + Ni_2O_3 \quad (9)$$

The results reveal that Ga^{3+} is the most favourable dopant at the Ni site (refer to Figure 5). Its solution enthalpy is 0.05 eV. The second most favourable dopant is Al^{3+} having the solution enthalpy

of 0.12 eV. We further predict that Fe^{3+} is also worth investigating as its solution enthalpy (0.14 eV) is very close to the solution enthalpies calculated for Ga^{3+} and Al^{3+}. The solution enthalpy for In_2O_3 is 1.17 eV. There is a reduction in the solution enthalpy for Sc_2O_3 though the ionic radius of Sc is larger than that of In. There is a gradual increase in the solution enthalpy from Y to La. As they exhibit relatively high solution enthalpies, they are highly unlikely to substitute the Ni.

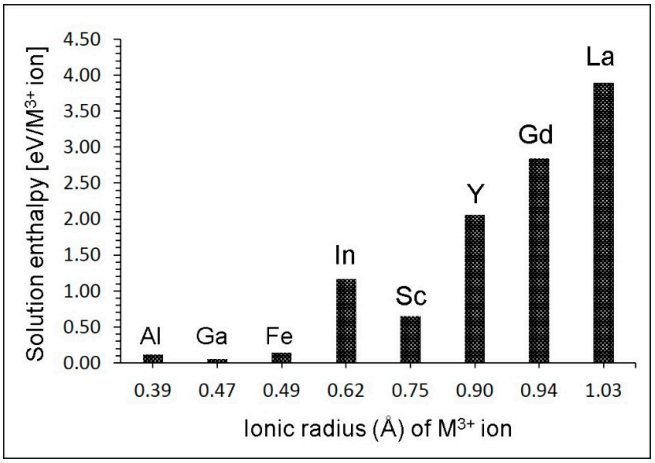

Figure 5. Solution enthalpies of trivalent dopants at the Ni site with respect to ionic radii.

3.6. Solution of Tetravalent Dopants

We also considered tetravalent dopants (M = Si, Ge, Ti, Sn, Zr, and Ce) at the Ni site. This process required the creation of Na vacancies according to the following reaction equation:

$$2MO_2 + 2Ni_{Ni}^{X} + 2Na_{Na}^{X} \rightarrow 2M_{Ni}^{\bullet} + 2V'_{Na} + Ni_2O_3 + Na_2O \quad (10)$$

The formation of Na vacancies would facilitate Na ion migration in this material. Figure 6 reports the solution enthalpies of MO_2. The promising candidate for this process is Ti^{4+} as this dopant exhibits the lowest solution enthalpy (+0.05 eV). As there is a very small enthalpy difference between the Ge^{4+}, and Ti^{4+}, Ge^{4+} can also be considered for experimental verification. High solution enthalpy for SiO_2 can be due to the smaller radius of Si^{4+} (0.40 Å) ion compared to that of Ni^{3+} (0.56 Å). Solution enthalpy increases with ionic radius from Sn to Ce. The highest solution enthalpy (5.38 eV) is observed for Ce implying it could be an important dopant only at high temperatures.

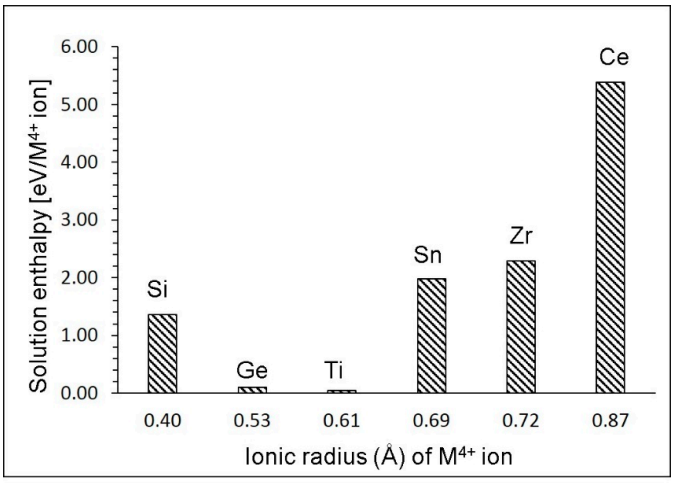

Figure 6. Solution enthalpies of tetravalent dopants at the Ni site with respect to ionic radii.

3.7. Diffusion of Na-Ion in the Presence of Dopants

Here we calculate the activation energies for Na-ion diffusion when promising dopants (Co^{2+}, Ga^{3+} and Ti^{4+}) are present on the Ni site. Figure 7 shows the energy profile diagrams for Na hops in each cases.

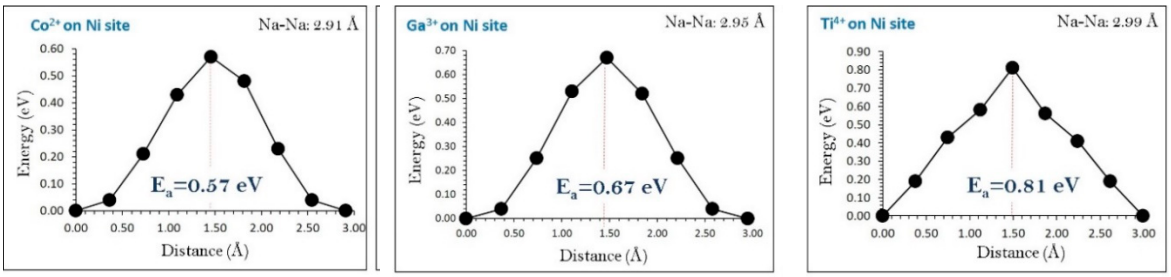

(**a**) (**b**) (**c**)

Figure 7. Energy profile diagrams for the Na local hop in the presence of favourable dopants (**a**) Co^{2+}, (**b**) Ga^{3+} and (**c**) Ti^{4+} on the Ni site.

In the case of Co^{2+} there is a reduction (by 0.10 eV) in the activation energy. This is due to the reduction in the Na-Na distance (2.91 Å) compared to that of pure crystal structure (2.95 Å). This perturbation in the distance can be due to the Co^{2+} occupying the Ni^{3+} (charge mismatch). Doping of Ga on the Ni site does not affect the activation energy as there is no change in the Na-Na distance. This is due to the similar charge (+3) of Ga and Ni. There is a slight elongation noted in the Na-Na distance when Ti^{4+} is present on the Ni site. This reflects in the increment of activation energy by 0.14 eV. The ionic radii of Ni^{3+}, Co^{2+}, Ga^{3+} and Ti^{4+} are 0.56 Å, 0.58 Å, 0.47 Å and 0.61 Å respectively. It is also noted that the contribution of ionic radius mismatch in the activation energy is less significant.

Considering the solution enthalpies and activation energies for the promising dopants, it is noted that Ga^{3+} doping at the Ti site is the most favourable as this dopant exhibits the lowest solution enthalpy of 0.05 eV and the same activation energy of 0.67 eV for Na-ion diffusion calculated in the un-doped $NaNiO_2$. The second most favourable dopant is Ti^{4+} as its solution enthalpy is 0.06 eV and this dopant increases the activation energy by 0.14 eV. Though there is a reduction in the activation energy (by 0.10 eV) upon Co^{2+} doping, the solution enthalpy is significantly high (3.89 eV) meaning that this dopant is not promising.

4. Conclusions

The present atomistic simulation study enabled us to gain insights into the defect chemistry, Na-ion diffusion pathways with activation energies, and dopant properties in $NaNiO_2$. The lowest energy defect is the Na-Ni anti-site, in which Na and Ni would exchange their positions at low concentration. The Na Frenkel is the second most favourable defect process. Long range Na-ion diffusion is in the *ab* plane with the activation energy of 0.67 eV. This suggests that there will be a significant Na-ion conduction in this material. Doping of Co^{2+} and Ti^{4+} at the Ni site would increase the concentration of Na interstitials and Na vacancies respectively. The most favourable isovalent dopant at the Ni site is Ga^{3+}. Considering the solution enthalpies and activation energies for the promising dopants, it is found that Ga^{3+} doping at the Ti site is the most favourable. This theoretical prediction should motivate future experimental work on this potentially important material.

Supplementary Materials: The following are available online at http://www.mdpi.com/1996-1073/12/16/3094/s1, Table S1: Interatomic potential parameters used in the atomistic simulations of $NaNiO_2$.

Author Contributions: Computation, R.K., N.K.; Writing, N.K.; Analysis and Editing, P.I. and A.C.

Funding: This research was financially supported by European Union's H2020 Programme under Grant Agreement no 824072–HARVESTORE.

Acknowledgments: We acknowledge Imperial College London and the University of Jaffna for providing computing facilities.

Conflicts of Interest: The authors declare no conflict of interest.

References

1. Armand, M.; Tarascon, J.M. Building better batteries. *Nature* **2008**, *451*, 652. [CrossRef] [PubMed]
2. Whittingham, M.S. Lithium Batteries and Cathode Materials. *Chem. Rev.* **2004**, *104*, 4271–4302. [CrossRef] [PubMed]
3. Padhi, A.K.; Nanjundaswamy, K.S.; Goodenough, J.B. Phospho-olivines as Positive-Electrode Materials for Rechargeable Lithium Batteries. *J. Electrochem. Soc.* **1997**, *144*, 1188–1194. [CrossRef]
4. Islam, M.S.; Fisher, C.A.J. Lithium and sodium battery cathode materials: Computational insights into voltage, diffusion and nanostructural properties. *Chem. Soc. Rev.* **2014**, *43*, 185–204. [CrossRef] [PubMed]
5. Masquelier, C.; Croguennec, L. Polyanionic (Phosphates, Silicates, Sulfates) Frameworks as Electrode Materials for Rechargeable Li (or Na) Batteries. *Chem. Rev.* **2013**, *113*, 6552–6591. [CrossRef] [PubMed]
6. Tarascon, J.M.; Armand, M. Issues and challenges facing rechargeable lithium batteries. *Nature* **2001**, *414*, 359. [CrossRef]
7. Jay, E.E.; Rushton, M.J.D.; Chroneos, A.; Grimes, R.W.; Kilner, J.A. Genetics of superionic conductivity in lithium lanthanum titanates. *Phys. Chem. Chem. Phys.* **2015**, *17*, 178–183. [CrossRef]
8. Recham, N.; Chotard, J.N.; Dupont, L.; Delacourt, C.; Walker, W.; Armand, M.; Tarascon, J.M. A 3.6 V lithium-based fluorosulphate insertion positive electrode for lithium-ion batteries. *Nat. Mater.* **2009**, *9*, 68. [CrossRef]
9. Islam, M.S.; Dominko, R.; Masquelier, C.; Sirisopanaporn, C.; Armstrong, A.R.; Bruce, P.G. Silicate cathodes for lithium batteries: Alternatives to phosphates? *J. Mater. Chem.* **2011**, *21*, 9811–9818. [CrossRef]
10. Clark, J.M.; Barpanda, P.; Yamada, A.; Islam, M.S. Sodium-ion battery cathodes $Na_2FeP_2O_7$ and $Na_2MnP_2O_7$: Diffusion behaviour for high rate performance. *J. Mater. Chem. A* **2014**, *2*, 11807–11812. [CrossRef]
11. Liu, Y.; Zhou, Y.; Zhang, J.; Xia, Y.; Chen, T.; Zhang, S. Monoclinic Phase Na_3Fe_2 $(PO_4)_3$: Synthesis, Structure, and Electrochemical Performance as Cathode Material in Sodium-Ion Batteries. *ACS Sustain. Chem. Eng.* **2017**, *5*, 1306–1314. [CrossRef]
12. Yabuuchi, N.; Kubota, K.; Dahbi, M.; Komaba, S. Research Development on Sodium-Ion Batteries. *Chem. Rev.* **2014**, *114*, 11636–11682. [CrossRef] [PubMed]
13. Hwang, J.-Y.; Myung, S.-T.; Sun, Y.-K. Sodium-ion batteries: Present and future. *Chem. Soc. Rev.* **2017**, *46*, 3529–3614. [CrossRef] [PubMed]
14. Kim, J.; Yoon, G.; Kim, H.; Park, Y.-U.; Kang, K. Na_3V $(PO_4)_2$: A New Layered-Type Cathode Material with High Water Stability and Power Capability for Na-Ion Batteries. *Chem. Mater.* **2018**, *30*, 3683–3689. [CrossRef]
15. Ellis, B.L.; Nazar, L.F. Sodium and sodium-ion energy storage batteries. *Curr. Opin. Solid State Mater. Sci.* **2012**, *16*, 168–177. [CrossRef]
16. Kuganathan, N.; Chroneos, A. Defect Chemistry and Na-Ion Diffusion in Na_3Fe_2 $(PO_4)_3$ Cathode Material. *Materials* **2019**, *12*, 1348. [CrossRef] [PubMed]
17. Kuganathan, N.; Chroneos, A. Defects, Dopants and Sodium Mobility in Na_2MnSiO_4. *Sci. Rep.* **2018**, *8*, 14669. [CrossRef]
18. Kuganathan, N.; Chroneos, A. Na_3V $(PO_4)_2$ cathode material for Na ion batteries: Defects, dopants and Na diffusion. *Solid State Ion.* **2019**, *336*, 75–79. [CrossRef]
19. Treacher, J.C.; Wood, S.M.; Islam, M.S.; Kendrick, E. Na_2CoSiO_4 as a cathode material for sodium-ion batteries: Structure, electrochemistry and diffusion pathways. *Phys. Chem. Chem. Phys.* **2016**, *18*, 32744–32752. [CrossRef]
20. Aparicio, P.A.; Dawson, J.A.; Islam, M.S.; De Leeuw, N.H. Computational Study of $NaVOPO_4$ Polymorphs as Cathode Materials for Na-Ion Batteries: Diffusion, Electronic Properties, and Cation-Doping Behavior. *J. Phys. Chem. C* **2018**, *122*, 25829–25836. [CrossRef]
21. Peters, J.; Buchholz, D.; Passerini, S.; Weil, M. Life cycle assessment of sodium-ion batteries. *Energy Environ. Sci.* **2016**, *9*, 1744–1751. [CrossRef]

22. Ong, S.P.; Chevrier, V.L.; Hautier, G.; Jain, A.; Moore, C.; Kim, S.; Ma, X.; Ceder, G. Voltage, stability and diffusion barrier differences between sodium-ion and lithium-ion intercalation materials. *Energy Environ. Sci.* **2011**, *4*, 3680–3688. [CrossRef]
23. Clément, R.J.; Bruce, P.G.; Grey, C.P. Review—Manganese-Based P2-Type Transition Metal Oxides as Sodium-Ion Battery Cathode Materials. *J. Electrochem. Soc.* **2015**, *162*, A2589–A2604. [CrossRef]
24. Kikkawa, S.; Miyazaki, S.; Koizumi, M. Deintercalated $NaCoO_2$ and $LiCoO_2$. *J. Solid State Chem.* **1986**, *62*, 35–39. [CrossRef]
25. Ma, X.; Chen, H.; Ceder, G. Electrochemical Properties of Monoclinic $NaMnO_2$. *J. Electrochem. Soc.* **2011**, *158*, A1307–A1312. [CrossRef]
26. Takeda, Y.; Nakahara, K.; Nishijima, M.; Imanishi, N.; Yamamoto, O.; Takano, M.; Kanno, R. Sodium deintercalation from sodium iron oxide. *Mater. Res. Bull.* **1994**, *29*, 659–666. [CrossRef]
27. Miyazaki, S.; Kikkawa, S.; Koizumi, M. Chemical and electrochemical deintercalations of the layered compounds $LiMO_2$ (M=Cr, Co) and $NaM'O_2$ (M′ Cr, Fe, Co, Ni). *Synth. Met.* **1983**, *6*, 211–217. [CrossRef]
28. Vassilaras, P.; Ma, X.; Li, X.; Ceder, G. Electrochemical Properties of Monoclinic $NaNiO_2$. *J. Electrochem. Soc.* **2013**, *160*, A207–A211. [CrossRef]
29. Seymour, I.D.; Chroneos, A.; Kilner, J.A.; Grimes, R.W. Defect processes in orthorhombic $LnBaCo_2O_{5.5}$ double perovskites. *Phys. Chem. Chem. Phys.* **2011**, *13*, 15305–15310. [CrossRef]
30. Rupasov, D.; Chroneos, A.; Parfitt, D.; Kilner, J.A.; Grimes, R.W.; Istomin, S.Y.; Antipov, E.V. Oxygen diffusion in $Sr_{0.75}Y_{0.25}CoO_{2.625}$: A molecular dynamics study. *Phys. Rev. B* **2009**, *79*, 172102. [CrossRef]
31. Fisher, C.A.J.; Hart Prieto, V.M.; Islam, M.S. Lithium Battery Materials $LiMPO_4$ (M=Mn, Fe, Co, and Ni): Insights into Defect Association, Transport Mechanisms, and Doping Behavior. *Chem. Mater.* **2008**, *20*, 5907–5915. [CrossRef]
32. Islam, M.S.; Driscoll, D.J.; Fisher, C.A.J.; Slater, P.R. Atomic-Scale Investigation of Defects, Dopants, and Lithium Transport in the $LiFePO_4$ Olivine-Type Battery Material. *Chem. Mater.* **2005**, *17*, 5085–5092. [CrossRef]
33. Kuganathan, N.; Islam, M.S. Li_2MnSiO_4 Lithium Battery Material: Atomic-Scale Study of Defects, Lithium Mobility, and Trivalent Dopants. *Chem. Mater.* **2009**, *21*, 5196–5202. [CrossRef]
34. Fisher, C.A.J.; Kuganathan, N.; Islam, M.S. Defect chemistry and lithium-ion migration in polymorphs of the cathode material Li_2MnSiO_4. *J. Mater. Chem. A* **2013**, *1*, 4207–4214. [CrossRef]
35. Armstrong, A.R.; Kuganathan, N.; Islam, M.S.; Bruce, P.G. Structure and Lithium Transport Pathways in Li_2FeSiO_4 Cathodes for Lithium Batteries. *J. Am. Chem. Soc.* **2011**, *133*, 13031–13035. [CrossRef]
36. Kuganathan, N.; Sgourou, E.N.; Panayiotatos, Y.; Chroneos, A. Defect Process, Dopant Behaviour and Li Ion Mobility in the Li_2MnO_3 Cathode Material. *Energies* **2019**, *12*, 1329. [CrossRef]
37. Kuganathan, N.; Kordatos, A.; Anurakavan, S.; Iyngaran, P.; Chroneos, A. Li_3SbO_4 lithium-ion battery material: Defects, lithium ion diffusion and tetravalent dopants. *Mater. Chem. Phys.* **2019**, *225*, 34–41. [CrossRef]
38. Kordatos, A.; Kuganathan, N.; Kelaidis, N.; Iyngaran, P.; Chroneos, A. Defects and lithium migration in Li_2CuO_2. *Sci. Rep.* **2018**, *8*, 6754. [CrossRef]
39. Kuganathan, N.; Chroneos, A. Defects and dopant properties of Li_3V_2 $(PO_4)_3$. *Sci. Rep.* **2019**, *9*, 333. [CrossRef]
40. Kuganathan, N.; Ganeshalingam, S.; Chroneos, A. Defects, Dopants and Lithium Mobility in Li_9V_3 $(P_2O_7)_3$ $(PO_4)_2$. *Sci. Rep.* **2018**, *8*, 8140. [CrossRef]
41. Kuganathan, N.; Kordatos, A.; Chroneos, A. Li_2SnO_3 as a Cathode Material for Lithium-ion Batteries: Defects, Lithium Ion Diffusion and Dopants. *Sci. Rep.* **2018**, *8*, 12621. [CrossRef]
42. Kuganathan, N.; Kordatos, A.; Chroneos, A. Defect Chemistry and Li-ion Diffusion in Li_2RuO_3. *Sci. Rep.* **2019**, *9*, 550. [CrossRef]
43. Kuganathan, N.; Kordatos, A.; Kelaidis, N.; Chroneos, A. Defects, Lithium Mobility and Tetravalent Dopants in the Li_3NbO_4 Cathode Material. *Sci. Rep.* **2019**, *9*, 2192. [CrossRef]
44. Kuganathan, N.; Kordatos, A.; Fitzpatrick, M.E.; Vovk, R.V.; Chroneos, A. Defect process and lithium diffusion in Li_2TiO_3. *Solid State Ion.* **2018**, *327*, 93–98. [CrossRef]
45. Kuganathan, N.; Tsoukalas, L.H.; Chroneos, A. Defects, dopants and Li-ion diffusion in Li_2SiO_3. *Solid State Ion.* **2019**, *335*, 61–66. [CrossRef]
46. Kuganathan, N.; Iyngaran, P.; Chroneos, A. Lithium diffusion in Li_5FeO_4. *Sci. Rep.* **2018**, *8*, 5832. [CrossRef]

47. Kuganathan, N.; Iyngaran, P.; Vovk, R.; Chroneos, A. Defects, dopants and Mg diffusion in $MgTiO_3$. *Sci. Rep.* **2019**, *9*, 4394. [CrossRef]
48. Tolchard, J.R.; Slater, P.R.; Islam, M.S. Insight into Doping Effects in Apatite Silicate Ionic Conductors. *Adv. Funct. Mater.* **2007**, *17*, 2564–2571. [CrossRef]
49. Gale, J.D.; Rohl, A.L. The General Utility Lattice Program (GULP). *Mol. Simul.* **2003**, *29*, 291–341. [CrossRef]
50. Gale, J.D. GULP: A computer program for the symmetry-adapted simulation of solids. *J. Chem. Soc. Faraday Trans.* **1997**, *93*, 629–637. [CrossRef]
51. Mott, N.F.; Littleton, M.J. Conduction in polar crystals. I. Electrolytic conduction in solid salts. *Trans. Faraday Soc.* **1938**, *34*, 485–499. [CrossRef]
52. Varotsos, P. Comparison of models that interconnect point defect parameters in solids with bulk properties. *J. Appl. Phys.* **2007**, *101*, 123503. [CrossRef]
53. Varotsos, P. Defect volumes and the equation of state in α-PbF_2. *Phys. Rev. B* **2007**, *76*, 092106. [CrossRef]
54. Varotsos, P. Point defect parameters in β-PbF_2 revisited. *Solid State Ion.* **2008**, *179*, 438–441. [CrossRef]
55. Kröger, F.A.; Vink, H.J. Relations between the Concentrations of Imperfections in Crystalline Solids. In *Solid State Physics*; Seitz, F., Turnbull, D., Eds.; Academic Press: Cambridge, MA, USA, 1956; Volume 3, pp. 307–435.
56. Nytén, A.; Abouimrane, A.; Armand, M.; Gustafsson, T.; Thomas, J.O. Electrochemical performance of Li_2FeSiO_4 as a new Li-battery cathode material. *Electrochem. Commun.* **2005**, *7*, 156–160. [CrossRef]
57. Politaev, V.V.; Petrenko, A.A.; Nalbandyan, V.B.; Medvedev, B.S.; Shvetsova, E.S. Crystal structure, phase relations and electrochemical properties of monoclinic Li_2MnSiO_4. *J. Solid State Chem.* **2007**, *180*, 1045–1050. [CrossRef]
58. Liu, H.; Choe, M.-J.; Enrique, R.A.; Orvañanos, B.; Zhou, L.; Liu, T.; Thornton, K.; Grey, C.P. Effects of Antisite Defects on Li Diffusion in $LiFePO_4$ Revealed by Li Isotope Exchange. *J. Phys. Chem. C* **2017**, *121*, 12025–12036. [CrossRef]
59. Kempaiah Devaraju, M.; Duc Truong, Q.; Hyodo, H.; Sasaki, Y.; Honma, I. Synthesis, characterization and observation of antisite defects in $LiNiPO_4$ nanomaterials. *Sci. Rep.* **2015**, *5*, 11041. [CrossRef]

© 2019 by the authors. Licensee MDPI, Basel, Switzerland. This article is an open access article distributed under the terms and conditions of the Creative Commons Attribution (CC BY) license (http://creativecommons.org/licenses/by/4.0/).